Applied Physics Letters

RESEARCH ARTICLE | SEPTEMBER 13 2011

Electroforming and endurance behavior of Al/$Pr_{0.7}Ca_{0.3}MnO_3$/Pt devices

Zhaoliang Liao; Peng Gao; Yang Meng; Hongwu Zhao; Xuedong Bai; Jiandi Zhang; Dongmin Chen

Appl. Phys. Lett. 99, 113506 (2011)
https://doi.org/10.1063/1.3638059

CrossMark

Articles You May Be Interested In

Low temperature solution-processed graphene oxide/$Pr_{0.7}Ca_{0.3}MnO_3$ based resistive-memory device

Appl. Phys. Lett. (July 2011)

Ferroelectricity-induced resistive switching in $Pb(Zr_{0.52}Ti_{0.48})O_3$/$Pr_{0.7}Ca_{0.3}MnO_3$/Nb-doped $SrTiO_3$ epitaxial heterostructure

Appl. Phys. Lett. (March 2012)

Thermally assisted resistive switching in $Pr_{0.7}Ca_{0.3}MnO_3$/Ti/$Ge_2Sb_2Te_5$ stack for nonvolatile memory applications

Appl. Phys. Lett. (August 2011)

03 September 2023 14:50:02

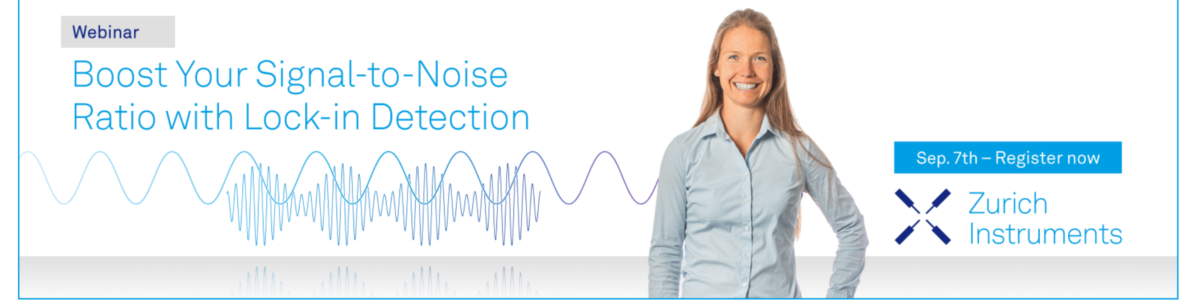

Electroforming and endurance behavior of $Al/Pr_{0.7}Ca_{0.3}MnO_3/Pt$ devices

Zhaoliang Liao,[1,2,a)] Peng Gao,[1] Yang Meng,[1] Hongwu Zhao,[1] Xuedong Bai,[1] Jiandi Zhang,[2] and Dongmin Chen[1,a)]

[1]*Beijing National Laboratory for Condensed Matter Physics, Institute of Physics, Chinese Academy of Sciences, Beijing 100190, China*
[2]*Department of Physics and Astronomy, Louisianan State University, Baton Rouge, Louisiana 70810, USA*

(Received 7 April 2011; accepted 24 August 2011; published online 13 September 2011)

We have investigated the electroforming (EF) and resistive switching (RS) of $Al/Pr_{0.7}Ca_{0.3}MnO_3$ (PCMO)/Pt devices by using high-resolution transmission electron microscopy and x-ray photoelectron spectroscopy combined with transport measurement. The device prefers EF with positive bias with respect to Pt electrode and their endurance is enhanced with the chemically reactive Al electrode. The presence of an $Al_2O_{3-\delta}$ layer in Al/PCMO junction indicates that the oxidization and reduction near the Al/PCMO interface play a key role in the RS. © *2011 American Institute of Physics*. [doi:10.1063/1.3638059]

03 September 2023 14:50:02

The resistive switching (RS) in metal/metal-oxide/metal (M/MO/M) heterostructure devices has been intensively studied for application as a non-volatile resistive random access memory (RRAM).[1–8] To date, the underlying physics for the key behavior of RRAM such as electroforming (EF) and endurance is still not well understood. In some cases, varying EF process[9] can significantly affect the characteristic of RS, while in other cases, EF process is not required.[10] The endurance, one of the critical attributes for practical application of RRAM, is yet to be improved in many of M/MO/M devices.[1] The role of the chemical reactivity of the electrodes is an important aspect of the working mechanism in these devices. It has been reported that for some MO materials,[11–13] the endurance of a device with reactive-metal (RM) top electrode (TE) and a non-reactive metal (NRM) bottom electrode (BE), RM/MO/NRM, is quite different from that with NRM TE, NRM/MO/NRM. Moreover, it has been observed that the fatigue is a serious problem in some of the NRM/MO/NRM as compared to RM/MO/NRM devices.[11–13] RM electrode appears to improve the endurance.[13–16] While the mechanism of RS is still under debate, it is generally accepted that the oxidation/reduction at the RM/MO interface plays a key role in RS.[11–16] The understanding of the role of RM electrode on RS and endurance is critical for making practical RRAM devices.

Here, we report the investigation of the EF and endurance behavior of $Al/Pr_{0.7}Ca_{0.3}MnO_3$ (PCMO) junction, where Al serves as a reactive TE. Much attention has been paid to PCMO for its remarkable RS performance.[3,16–23] By analyzing the evolution of the current-voltage (*I*-*V*) curves and cross-section structure of the Al/PCMO interface, we gain good insight into the nature of EF, endurance behavior, and the role of the RM electrode.

A 125 nm polycrystalline PCMO thin film was fabricated on a Pt (111) layer through a special low temperature (<400 °C) back-biased-face-target-sputtering process.[16] In order to prevent oxidization of Al TE, the Al film of ~3 nm deposited on the as-grown PCMO thin film was capped with 90 nm Pt by magnetron sputtering at room temperature. An array of 200 μm × 200 μm electrodes was subsequently patterned by a standard photolithography and reactive ion etching technique. All patterned devices were made to have the same thicknesses for the material stack. The electrical properties of the devices were characterized by means of *I*-*V* sweep using Keithley-2400 with Pt BE being grounded.

Figure 1(a) presents the first EF *I*-*V* curves of different Al/PCMO/Pt devices with several maximum voltages, $0 \rightarrow +V_{max} \rightarrow -V_{max} \rightarrow 0$, respectively. The *I*-*V* curves exhibit hysteresis only when V_{max} reaches a threshold value. As shown in the inset of Fig. 1(a), no *I*-*V* hysteresis has been observed for $V_{max} \leq 1.2$ V. Through the extrapolation of our data, this threshold voltage for effective EF is found to be ~1.5 V which is directly related to the current peak position ($V_p = 1.5$ V) in the *I*-*V* loops [see Fig. 1(a)], reflecting the presence of an activation barrier for EF. In order to gain more insight into the EF as well as RS behavior, we applied only positive sweep loops ($0 \rightarrow V_{max} \rightarrow 0$) successively with gradually increasing V_{max} for a given device. First, we notice that after the initial EF at a V^1_{max}, subsequent positive voltage sweep loop does not exhibit hysteresis for $V_{max} \leq V^1_{max}$ (the red curve overlaying the return trace of the 1st *I*-*V* in black in Fig. 1(b)). However, hysteresis reappears when the V_{max} exceeds V^1_{max} and increases sequentially to V^2_{max} and

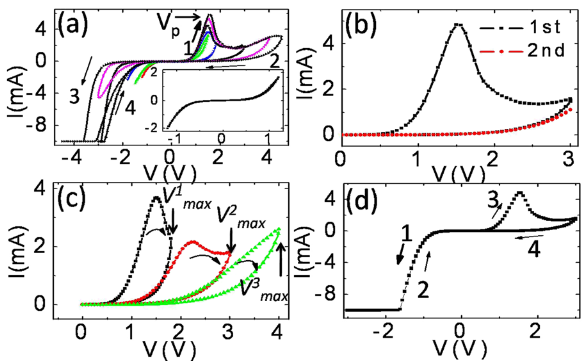

FIG. 1. (Color online) RS characteristics of the Al/PCMO/Pt memory devices: (a) The EF with different sweep voltages with the inset showing no hysteresis when $V < 1.5$ V; (b) Consecutive *I*-*V* sweep loops ($0 \rightarrow V_{max} \rightarrow 0$) $V_{max} = 3$ V; (c) Sequential *I*-*V* sweep loops ($0 \rightarrow V_{max} \rightarrow 0$) with $V^1_{max} = 1.8$ V, $V^2_{max} = 3$ V, $V^3_{max} = 4$ V; and (d) *I*-*V* sweep loop ($0 \rightarrow -3$ V $\rightarrow 3$ V $\rightarrow 0$). Arrows and number indicate sweep direction and sequence.

a)Authors to whom correspondence should be addressed. Electronic addresses: zliao1@tigers.lsu.edu and dmchen@aphy.iphy.ac.cn.

V^3_{max} (see Fig. 1(c)). Furthermore the threshold voltage of EF (V_p) increases with each additional cycle of voltage ramp at higher V_{max} than its previous cycle, indicating that the resistance state or RS barrier can be tuned with maximum EF voltage. On the other hand, for an as-fabricated device, if the initial sweep voltage polarity is reversed to 0 → −3 V → 3 V → 0, there is no *I-V* hysteresis at negative bias as shown in Fig. 1(d). When the negative applied voltage is increased further by removing the current compliance, a permanent breakdown due to large joule heating will occur. Therefore, we concluded that EF only occurs in the initial positive bias ramp for Al/PCMO/Pt devices.

For a given device, RS behavior is uniquely determined by the EF process. As long as the switching voltage does not exceed the maximum EF voltage (V_{max}), the device can be cycled between SET (from a high resistance state (HRS) to a low resistance state (LRS)) and RESET (from LRS to HRS).[16] As shown in Fig. 2(a) for a device with EF at $V_{max} = 3.0$ V, some degrees of fatigue are evident as the hysteresis loop changes during the initial cycles, reflecting the imbalance between SET and RESET processes. However, after few initial cycles of SET/RESET, the *I-V* hysteresis loop becomes repeatable, clearly indicating that the device reaches a balance between SET and RESET. This is in contrast to the hysteresis characteristics in the devices made with NRM TE.[16] We have also examined the endurance of the devices by monitoring the pulse switching of the resistance states up to $\sim 10^{10}$ cycles and found no obvious degradation of HRS and LRS.[21]

With this setup of devices, we are able to tune the working resistance difference between HRS and LRS by simply changing SET voltage $V^{(-)}_{max}$ (at negative sweep, 0 → $V^{(-)}_{max}$ → 0) and RESET voltage $V^{(+)}_{max}$ (at positive sweep 0 → $V^{(+)}_{max}$ → 0). For example, we successively swept the device (i.e., 0 → $V^{(+)}_{max}$ → $V^{(-)}_{max}$ → 0) with different ratios of $V^{(-)}_{max}/V^{(+)}_{max}$ after a single EF and then recorded the resistances of both HRS and LRS at a read voltage $V^{(-)}_{max} < V_r < 0$. Fig. 2(b) shows the data for 6 sets of $V^{(-)}_{max}/V^{(+)}_{max}$ with 9 sweeps carried out for each and the HRS and LRS recorded at $V_r = -2.1$ V. The first sweep, −3 V/3 V is the initial EF. For each $V^{(-)}_{max}/V^{(+)}_{max}$, the resistances settle to stable values after several cycles of voltage sweep, indicating that the device is able to quickly reestablish a balance after it being set to an another level. Indeed, we have performed the endurance test up to $\sim 10^{10}$ cycles for different bias conditions and found that a SET/RESET balance can be always achieved with excellent endurance. These results suggest that the working resistance states can be tuned sequentially and effectively for these devices.

It has been proposed that Al/PCMO interface plays an important role in the RS.[16] To reveal the nature of the interface, we have investigated the cross-section structure of Al/PCMO/Pt with high resolution transmission electron microscopy (HRTEM). Interestingly, HRTEM image reveals a ∼4.7 nm thick amorphous layer [see Fig. 3(a)] at the interface between Al and 125 nm thick PCMO film. We further examined a 19 nm thick PCMO film capped with the same thickness of Al layer and found no change in the thickness of amorphous layer [see Fig. 3(b)]. Comparing with the same thickness of PCMO film capped with a glue layer of Fig. 3(c), it is clear that a portion of the PCMO layer should become amorphous (α-PCMO) after Al capping. In addition, x-ray photoelectron spectroscopy (XPS) of the Al 2p core level taken near the Al electrode (Fig. 3(d)) shows both metal Al 2p (at ∼72 eV) and oxidized Al 2p (∼75 eV) peaks, suggesting partial oxidization of Al electrode and formation of $Al_2O_{3-\delta}$ at the interface. Yasuhara *et al.*[22] also reported a similar observation and suggested that a ∼1 nm thick $Al_2O_{3-\delta}$ layer was formed at the Al/PCMO interface. Thus, the structure of our device is actually $Al/Al_2O_{3-\delta}$/α-PCMO/PCMO/Pt. It is suggested that the formation of the α-PCMO layer is the consequence of the loss of oxygen to the top reactive electrode.[19] From the relative thickness of 1 nm Al_2O_3 vs. 4 nm α-PCMO, the oxygen vacancies concentration in the α-PCMO is estimated to be ∼34%. Therefore, the spontaneous formation of oxygen-deficient $Al_2O_{3-\delta}$ and α-PCMO at the interface is the essential aspect of this device.

The oxygen migration at the Al/PCMO interface and the redox reaction of the interface layer are thus critical for the RS in Al/PCMO/Pt devices. The *oxidation* (RESET) of the Al electrode, extraction of oxygen ions from PCMO

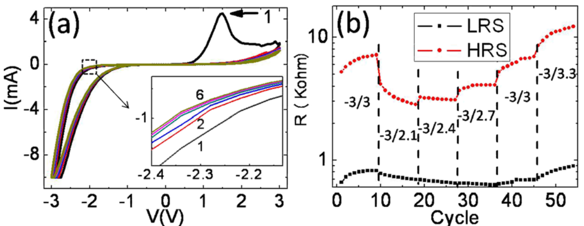

FIG. 2. (Color online) (a) Consecutive *I-V* sweeps after EF with $V_{max} = 3.0$ V. Inset shows the zoom-in of the marked region of *I-V* curves of 6-sequencial loops. Label-1 marks the first loop (EF). (b) 6 groups of HRS and LRS are distinguished by the vertical dash line and the corresponding sweep parameter $V^{(-)}_{max}/V^{(+)}_{max}$ is indicated for each group. Resistance state was read at $V_r = -2.1$ V.

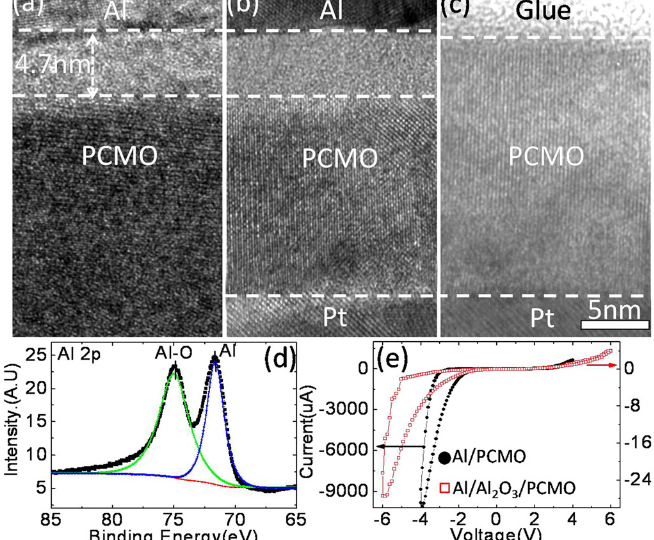

FIG. 3. (Color online) HRTEM images (with the same scale bar) of Al/PCMO/Pt device cross section: (a) 125 nm thick PCMO; (b) 19 nm thick PCMO. (c) HRTEM image of 19 nm thick PCMO without Al layer. (d) XPS spectra of Al 2p core level showing distinct oxidization state. (e) *I-V* characteristics for electroformed Al/PCMO/Pt (solid circular dot curve) and as fabricated Al/Al_2O_3/PCMO/Pt (hollow square curve).

03 September 2023 14:50:02

under positive bias, and its *reduction* (SET), migration of oxygen ions from $Al_2O_{3-\delta}$ back to PCMO under negative bias, occur alternatively at the Al/PCMO junction forming the characteristic RS. The thickness of $Al_2O_{3-\delta}$ may change, but the secondary-ion mass spectrometry analyses indicate that oxygen migration mainly changes the relative oxygen content in $Al_2O_{3-\delta}$.[23] In general, the SET and RESET should be asymmetric since oxidation is much easier in aluminum oxide than its reduction. However, the resistance of $Al_2O_{3-\delta}$ will increase during RESET, such that more voltage drops across $Al_2O_{3-\delta}$ layer and less across PCMO; as a result, it is harder for oxygen ions to migrate from PCMO to $Al_2O_{3-\delta}$, and further oxidation in $Al_2O_{3-\delta}$ becomes limited.[24] On the other hand, during SET, the large initial voltage drop on in $Al_2O_{3-\delta}$ will facilitate oxygen migration from $Al_2O_{3-\delta}$ into PCMO, but reduction of $Al_2O_{3-\delta}$ becomes harder as the layer becomes more conductive with increasing oxygen vacancies. There is no quantitative data yet on the redox reaction kinetics of $Al_2O_{3-\delta}$/PCMO interface. However, for perovskite $SrTi_{1-x}Fe_xO_{3-\delta}$, Steinsvik *et al.*[25] found that the activation enthalpy for annihilation of oxygen vacancies decreases from 2.0 eV to -0.2 eV with δ increasing from 0 to 0.4. In other words, it will be increasingly difficult to create oxygen vacancies (reduction) in a sample with a higher degree of oxygen deficiency. Likewise for $Al_2O_{3-\delta}$, the degree of difficulty in oxidization (or, reduction) will decrease (or, increase) with increasing δ. Therefore, both the electric field distribution and the kinetics of the redox reaction at the interface naturally self-limit the process and create the balance between SET and RESET.

Based on the above scenario, the EF and the SET/RESET cycles can be qualitatively understood. To drive oxygen migration between PCMO and $Al_2O_{3-\delta}$ and cause reduction/oxidation, the electric field should overcome the kinetic barrier of interface reduction/oxidation. Initially, because of rich oxygen vacancies in the $Al_2O_{3-\delta}$ layer, oxygen ions incline to migrate to the $Al_2O_{3-\delta}$ from PCMO, thus EF occurs at positive bias. The activation barrier increases as the oxygen vacancies in the $Al_2O_{3-\delta}$ layer are depleted with successive EF, hence, the current peak shifts to higher bias in Fig. 1(c). Furthermore, the SET/RESET balance will depend on the history of relative oxygen vacancy concentration between $Al_2O_{3-\delta}$ and PCMO. For each SET/RESET parameter, $V^{(-)}{}_{max}/V^{(+)}{}_{max}$, the device can adjust the relative level of oxygen concentration by the self-limiting process at the interface through a few SET/RESET cycles and eventually reach a balance as shown in Fig. 2(b).

To further test the above mechanism, we have deposited a 3 nm stoichiometric Al_2O_3 layer on the top of PCMO by atomic layer deposition at 250 °C. Indeed the as fabricated Al/Al_2O_3/PCMO/Pt devices can yield reproducible RS without EF as shown in Fig. 3(e). The Al/Al_2O_3/PCMO/Pt devices exhibit similar *I-V* hysteresis to that of electroformed Al/PCMO/Pt ones but require larger negative bias to SET (reduce) Al_2O_3 due to more stable initial phase of Al oxide. The better insulation and fewer oxygen vacancies in the Al_2O_3 layer also result in a much larger resistance of Al/Al_2O_3/PCMO/Pt than that of Al/PCMO/Pt device.

In summary, we have revealed important characteristics of the EF and RS of Al/PCMO/Pt devices. The redox reaction at the interface between reactive Al electrode and PCMO layer plays a key role in the EF and RS. In particular, a self-limited field-induced oxygen migration leads to a balance between oxidization/reduction during SET/RESET cycles. Our results demonstrate the advantage of using a reactive metal electrode for improving the functionality of the metal oxide based memory devices.

This work was supported by a grant from the Chinese Academy of Sciences (NO. KJCX2-SW-W26) and also by the National Natural Science Foundation of China under Grant No.90406017. ZL was partially supported by U.S. DOE under Grant No. DOE DE-SC0002136. We thank 4DS Inc. for supplying the PCMO films and for their invaluable discussions.

[1]R. Waser and M. Aono, Nature Mater. **6**, 833 (2007); A. Sawa, Mater. Today **11**, 28 (2008), and references therein.
[2]T. W. Hickmott, J. Appl. Phys. **33**, 2669 (1962).
[3]S. Q. Liu, N. J. Wu, and A. Ignatiev, Appl. Phys. Lett. **76**, 2749 (2000).
[4]A. Beck, J. G. Bednorz, Ch. Gerber, C. Rossel, and D. Widmer, Appl. Phys. Lett. **77**, 139 (2000).
[5]S. Seo, B. H. Park, D. H. Seo, E. J. Jeoung, D.-S. Suh, Y. S. Joung, I. K. Yoo, I. R. Hwang, S. H. Kim, I. S. Byun, J.-S. Kim, J. S. Choi, and B. H. Park, Appl. Phys. Lett. **85**, 5655 (2004).
[6]B. J. Choi, D. S. Jeong, S. K. Kim, C. Rohde, S. Choi, J. H. Oh, H. J. Kim, C. S. Hwang, K. Szot, R. Waser, B. Reichenberg, and S. Tiedke, J. Appl. Phys. **98**, 033715 (2005).
[7]X. Chen, N. J. Wu, J. Strozier, and A. Ignatiev, Appl. Phys. Lett. **89**, 063507 (2006).
[8]A. Odagawa, Y. Katoh, Y. Kanzawa, Z. Wei, T. Mikawa, S. Muraoka, and T. Takagi, Appl. Phys. Lett. **91**, 133503 (2007).
[9]F. Gomez-Marlasca, N. Ghenzi, M. J. Rozenberg, and P. Levy, Appl. Phys. Lett. **98**, 042901 (2011)
[10]R. Meyer, L. Schloss, J. Brewer, R. Lambertson, W. Kinney, J. Sanchez, and D. Rinerson, "Oxide dual-layer memory element for scalable nonvolatile cross-point memory technology," in *Proceedings of the Non-Volatile Memory Technology Symposium* (IEEE, 2008), pp. 1–5.
[11]H. B. Lv, M. Wang, H. J. Wan, Y. L. Song, W. J. Luo, P. Zhou, T. G. Tang, Y. Y. Lin, R. Huang, S. Song, J. G. Wu, H. M. Wu, and M. H. Chi, Appl. Phys. Lett. **94**, 213502 (2009).
[12]W. Shen, R. Dittmann, U. Breuer, and R. Waser, Appl. Phys. Lett. **93**, 222102 (2008).
[13]R. Yang and X. M. Li, Phys. Status Solidi A **208**, 1041 (2011).
[14]C. Y. Lin, C. Y. Wu, C. Y. Wu, T. Y. Tseng, and C. Hu, J. Appl. Phys. **102**, 094101 (2007).
[15]M. Hasan, R. Dong, H. J. Choi, D. S. Lee, D. J. Seong, M. B. Pyun, and H. Hwang, Appl. Phys. Lett. **92**, 202102 (2008).
[16]Z. L. Liao, Z. Z. Wang, Y. Meng, Z. Y. Liu, P. Gao, J. L. Gang, H. W. Zhao, X. J. Liang, X. D. Bai, and D. M. Chen, Appl. Phys. Lett. **94**, 253503 (2009).
[17]A. Sawa, T. Fujii, M. Kawasaki, and Y. Tokura, Appl. Phys. Lett. **85**, 4073 (2004).
[18]K. Shono, H. Kawano, T. Yokota, and M. Gomi, Appl. Phys. Express **1**, 055002 (2008).
[19]H. Kawano, K. Shono, T. Yokota, and M. Gomi, Appl. Phys. Express **1**, 101901 (2008).
[20]K. Tsubouchi, I. Ohkubo, H. Kumigashira, M. Oshima, Y. Matsumoto, K. Itaka, T. Ohnishi, M. Lippmaa, and H. Koinuma, Adv. Mater. **19**, 1711 (2007).
[21]Z. Z. Wang, Z. L. Liao, P. Gao, X. D. Bai, and D. M. Chen, "Non-volatile resistive switching of $Pr_{0.7}Ca_{0.3}MnO_3$ films prepared at low temperature" (unpublished).
[22]R. Yasuhara, T. Yamamoto, I. Ohkubo, H. Kumigashira, and M. Oshima, Appl. Phys. Lett. **97**, 132111 (2010).
[23]D. J. Seong, M. Hassan, H. J. Choi, J. Y. Lee, J. S. Yoon, J. B. Park, W. T. Lee, M. S. Oh, and H. S. Hwang, IEEE Electron Device Lett. **30**, 919 (2009).
[24]S. K. R. S. Sankaranarayanan, E. Kaxiras, and S. Ramanathan, Phys. Rev. Lett. **102**, 095504 (2009).
[25]S. Steinsvik, R. Bugge, J. Gjønnes, J. Taftø, and T. Norby, J. Phys. Chem. Solids **58**, 969 (1997).

03 September 2023 14:50:02